doi:10.1093/jmcb/mjaa075
Published online January 2, 2021

Article

Observation of an α-synuclein liquid droplet state and its maturation into Lewy body-like assemblies

Maarten C. Hardenberg[1], Tessa Sinnige[1,5], Sam Casford[1], Samuel T. Dada[1], Chetan Poudel[2], Elizabeth A. Robinson[1], Monika Fuxreiter[3], Clemens F. Kaminksi[2], Gabriele S. Kaminski Schierle[2], Ellen A. A. Nollen[4], Christopher M. Dobson[1], and Michele Vendruscolo [1,*]

[1] Centre for Misfolding Diseases, Department of Chemistry, University of Cambridge, Cambridge CB2 1EW, UK
[2] Department of Chemical Engineering and Biotechnology, University of Cambridge, Cambridge CB3 0AS, UK
[3] MTA-DE Laboratory of Protein Dynamics, Department of Biochemistry and Molecular Biology, University of Debrecen, Hungary
[4] European Research Institute for the Biology of Aging, University Medical Center Groningen, University of Groningen, Groningen 9713 AV, The Netherlands
[5] Present address: Bijvoet Centre for Biomolecular Research, Department of Chemistry, Utrecht University, Utrecht 3584 CH, The Netherlands
* Correspondence to: Michele Vendruscolo, E-mail: mv245@cam.ac.uk

Edited by Xuebiao Yao

Misfolded α-synuclein is a major component of Lewy bodies, which are a hallmark of Parkinson's disease (PD). A large body of evidence shows that α-synuclein can aggregate into amyloid fibrils, but the relationship between α-synuclein self-assembly and Lewy body formation remains unclear. Here, we show, both *in vitro* and in a *Caenorhabditis elegans* model of PD, that α-synuclein undergoes liquid–liquid phase separation by forming a liquid droplet state, which converts into an amyloid-rich hydrogel with Lewy-body-like properties. This maturation process towards the amyloid state is delayed in the presence of model synaptic vesicles *in vitro*. Taken together, these results suggest that the formation of Lewy bodies may be linked to the arrested maturation of α-synuclein condensates in the presence of lipids and other cellular components.

Keywords: α-synuclein, liquid–liquid phase separation, Parkinson's disease

Introduction

Parkinson's disease (PD) is the most common neurodegenerative movement disorder, affecting about 2% of the world population over 65 years of age (Dawson and Dawson, 2003; Poewe et al., 2017). The molecular origins of this disease are not fully understood, although they have been closely associated with the aberrant aggregation of α-synuclein (Polymeropoulos et al., 1997; Dawson and Dawson, 2003; Singleton et al., 2003), a disordered protein whose function appears to involve the regulation of synaptic vesicle trafficking (Burré et al., 2010; Bendor et al., 2013; Fusco et al., 2016; Lautenschläger et al., 2018). This gap in our knowledge of the disease aetiology makes it difficult to choose a target for drug discovery and it is therefore partly responsible for the current lack of disease-modifying therapies for PD (Schapira et al., 2014; Dehay et al., 2015; Valera and Masliah, 2016; Brundin et al., 2017).

Received July 22, 2020. Revised October 9, 2020. Accepted October 29, 2020.

The pathological hallmark of PD is the presence of Lewy bodies within dopaminergic neurons in the brains of affected patients (Goedert et al., 2017). Although misfolded α-synuclein is a principal constituent of Lewy bodies (Spillantini et al., 1997, 1998), ultrastructural and proteomic studies have indicated that these aberrant deposits contain a plethora of other cellular components, including lipid membranes and organelle fragments (Arima et al., 1998; Spillantini et al., 1998; Wakabayashi et al., 2013; Shahmoradian et al., 2019; Mahul-Mellier et al., 2020). These findings have led to the suggestion that the processes associated with the formation of Lewy bodies could be major drivers of neurotoxicity in PD (Wakabayashi et al., 2013; Davis, 2020; Mahul-Mellier et al., 2020).

Since it has also been shown that α-synuclein can aggregate into ordered amyloid fibrils *in vitro* (Knowles et al., 2009; Cohen et al., 2011; Cremades et al., 2012; Iljina et al., 2016; Li et al., 2018) and *in vivo* (Ko et al., 2008; Van Ham et al., 2008; Taschenberger et al., 2012; Volpicelli-Daley et al., 2014; Visanji et al., 2016; Schweighauser et al., 2020), we asked how such α-synuclein aggregation can be reconciled with the formation of highly complex and heterogeneous assemblies such as Lewy bodies. We hypothesized that α-synuclein may be

capable of irreversibly capturing cellular components through liquid–liquid phase separation, as this mechanism has been shown to drive the self-assembly of various disease-associated proteins on pathway to the formation of solid aggregates (Hyman et al., 2014; Banani et al., 2017; Shin and Brangwynne, 2017; Boeynaems et al., 2018). Under healthy conditions, the condensation of proteins into a dense liquid droplet state through liquid–liquid phase separation is normally reversible and exploited in a variety of ways to carry out cellular functions, including RNA metabolism, ribosome biogenesis, DNA damage response, and signal transduction (Ader et al., 2010; Hyman et al., 2014; Banani et al., 2017). Upon dysregulation, however, liquid droplets can mature into gel-like deposits, which irreversibly sequester essential cellular components and lead to pathological processes (Patel et al., 2015). This phenomenon has been observed for FUS and TDP-43 in amyotrophic lateral sclerosis (Murakami et al., 2015; Patel et al., 2015) and for tau in Alzheimer's disease (Ambadipudi et al., 2017; Wegmann et al., 2018; Kanaan et al., 2020). Our results show that α-synuclein can undergo a similar process by forming a dense liquid droplet state, which matures into a gel-like state rich in amyloid structure, consistent with recent results (Ray et al., 2020).

Results

α-synuclein forms non-amyloid inclusions in C. elegans

To understand the initial events in the α-synuclein aggregation process, we assessed its self-association using confocal fluorescence lifetime imaging (FLIM) in the nematode worm *C. elegans*. The fluorescence lifetime of a fluorophore has been previously shown to be an accurate measure of protein self-assembly and amyloid formation, both *in vitro* and in *C. elegans*, and allows amyloid formation to be tracked independent of protein concentration or fluorescence intensity (Kaminski Schierle et al., 2011; Laine et al., 2019; Poudel et al., 2020). Given the optical transparency and well-established genetics of *C. elegans*, we sought to compare the fluorescence lifetime of a human α-synuclein–yellow fluorescent protein (YFP) fusion protein stably expressed in body wall muscle cells (OW40 worm model, see Materials and methods). As worms do not express native α-synuclein, this model enabled us to specifically study the self-association of human α-synuclein in a cellular context and at known concentrations (± 200–300 μM) (Supplementary Figure S1; Materials and methods). In line with previous reports (Van Ham et al., 2008), we observed age-dependent coalescence of α-synuclein–YFP into distinct cytoplasmic inclusions at body wall muscle cells (Figure 1A; Supplementary Figure S2). Next, we performed high-resolution FLIM to be able to differentiate the fluorescence lifetime of proteins localized at inclusions from the diffuse (non-aggregated) pool (Figure 1A). Our analysis revealed that the self-association state of α-synuclein–YFP in inclusions was similar to that of the diffuse state for the majority of the nematode's adult life (Days 1–11 of adulthood), indicating that the early α-synuclein assemblies are predominantly non-amyloid in *C. elegans* (Figure 1B and C). Only at old age, α-synuclein–YFP inclusions started to show increased amyloid-like features (Days 13–15 of adulthood), an observation supported by the simultaneous appearance of proteinase K-resistant protein species (Figure 1D). In addition to the presence of amyloid features, we found that the majority of inclusions at old age (Day 15) were immunoreactive for ubiquitin, which is characteristic of α-synuclein deposits in PD (Figure 2A–C). By contrast, ubiquitin is not found in inclusions of younger animals (Day 7). This is expected, as post-translational modifications, such as ubiquitination, occur later on in PD pathogenesis, and indicates the presence of aggregated α-synuclein species (Mahul-Mellier et al., 2020). Together, our FLIM analysis shows that α-synuclein predominantly resides in mobile, non-amyloid inclusions, which is in agreement with previous studies (Van Ham et al., 2008; Kaminski Schierle et al., 2011; Laine et al., 2019; Poudel et al., 2020), before transitioning into amyloid and ubiquitin-positive deposits.

Early α-synuclein inclusions in C. elegans have liquid-like properties

The presence of non-amyloid α-synuclein assemblies in *C. elegans* prompted us to further investigate their material properties. To this end, we used the aliphatic alcohol 1,6-hexanediol, which has recently been used as a tool to test the liquid properties of protein condensates *in vitro* as well as *in vivo* (Kroschwald et al., 2017). Hexanediol dissolves assemblies maintained by weak hydrophobic interactions, whereas solid-like amyloid structures remain intact. Exposure to 10% (*w*/*v*) hexanediol in *C. elegans* almost completely dissolved α-synuclein inclusions between Days 1 and 11 of adulthood, reflecting the role of low-affinity interactions in inclusion assembly (Figure 3A and B; Supplementary Movie S1). As before, inclusions in aged nematodes (Days 13–15 of adulthood) appeared to be amyloid-like, as evidenced by decreased hexanediol-mediated dissipation. We then assessed whether α-synuclein assemblies in younger nematodes could reappear after hexanediol was washed out. Indeed, newly formed small inclusions were observed in washed worms after one day of recovery, reflecting the dynamic and liquid-like properties of α-synuclein assemblies in *C. elegans* (Figure 3C and D). To validate our observations, we tested the liquid properties of α-synuclein assemblies using fluorescence recovery after photobleaching (FRAP) (Figure 3E–G). We found that α-synuclein at inclusions was liquid up until Day 11 of adulthood, as evidenced by rapid recovery after photobleaching. Further ageing, however, resulted in a decline in FRAP, which confirms the observed transition from liquid to solid-like α-synuclein inclusions.

Liquid–liquid phase separation drives α-synuclein droplet formation in vitro

The results presented above indicate that α-synuclein is a component of liquid-like assemblies in *C. elegans*. To investigate whether this behaviour is mediated by the intrinsic

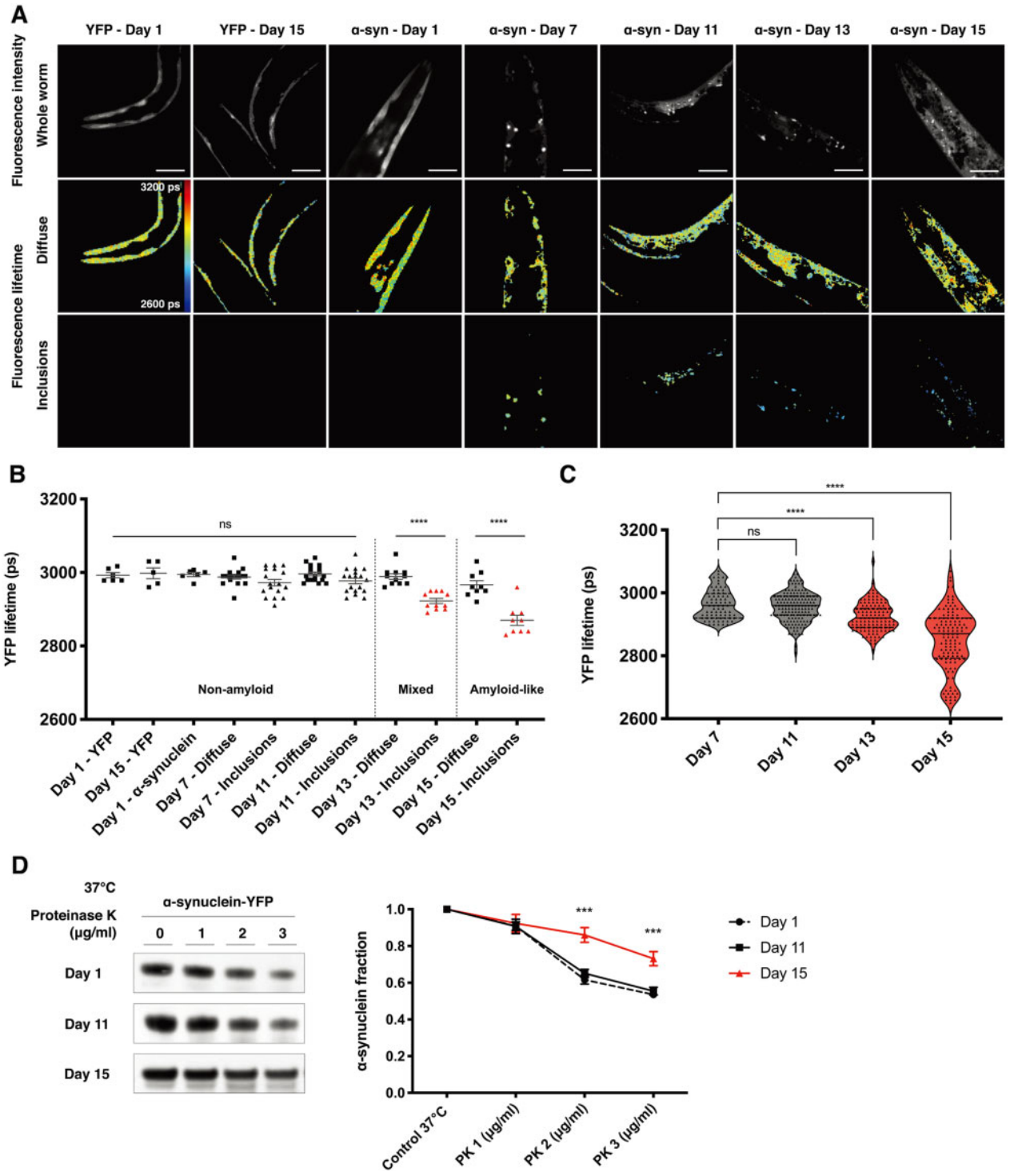

Figure 1 α-synuclein forms non-amyloid inclusions in *C. elegans*. (**A**) Age-dependent coalescence of α-synuclein–YFP in body wall muscle cells into cytoplasmic inclusions, with distinct lifetime profiles between inclusions and diffuse signal. Scale bar, 25 μm; rainbow scale bar, 2600 (blue)–3200 (red) picoseconds (ps). (**B**) Analysis of the high-resolution FLIM revealing that α-synuclein assemblies are predominantly non-amyloid in *C. elegans*. On Days 13 and 15, a shift towards lifetimes associated with the amyloid-state can be observed. No shift can be observed for worms expressing only YFP. Each square or triangle represents one animal from the population. (**C**) Violin plots for all individual inclusions from the animals in **B**. A distinct population of lower lifetime inclusions appears at old age. Black line: median. Dotted line: quartiles. (**D**) Appearance of proteinase K-resistant protein species showing α-synuclein–YFP with increased amyloid-like self-association in aged animals (Days 13–15 of adulthood). α-synuclein probed with the LB509 antibody (left) and quantification of protein levels corrected for loading control and normalized against untreated control (right) are shown. Results are mean ± SEM. One-way ANOVA; ***$P \leq 0.001$; ****$P \leq 0.0001$; ns, not significant.

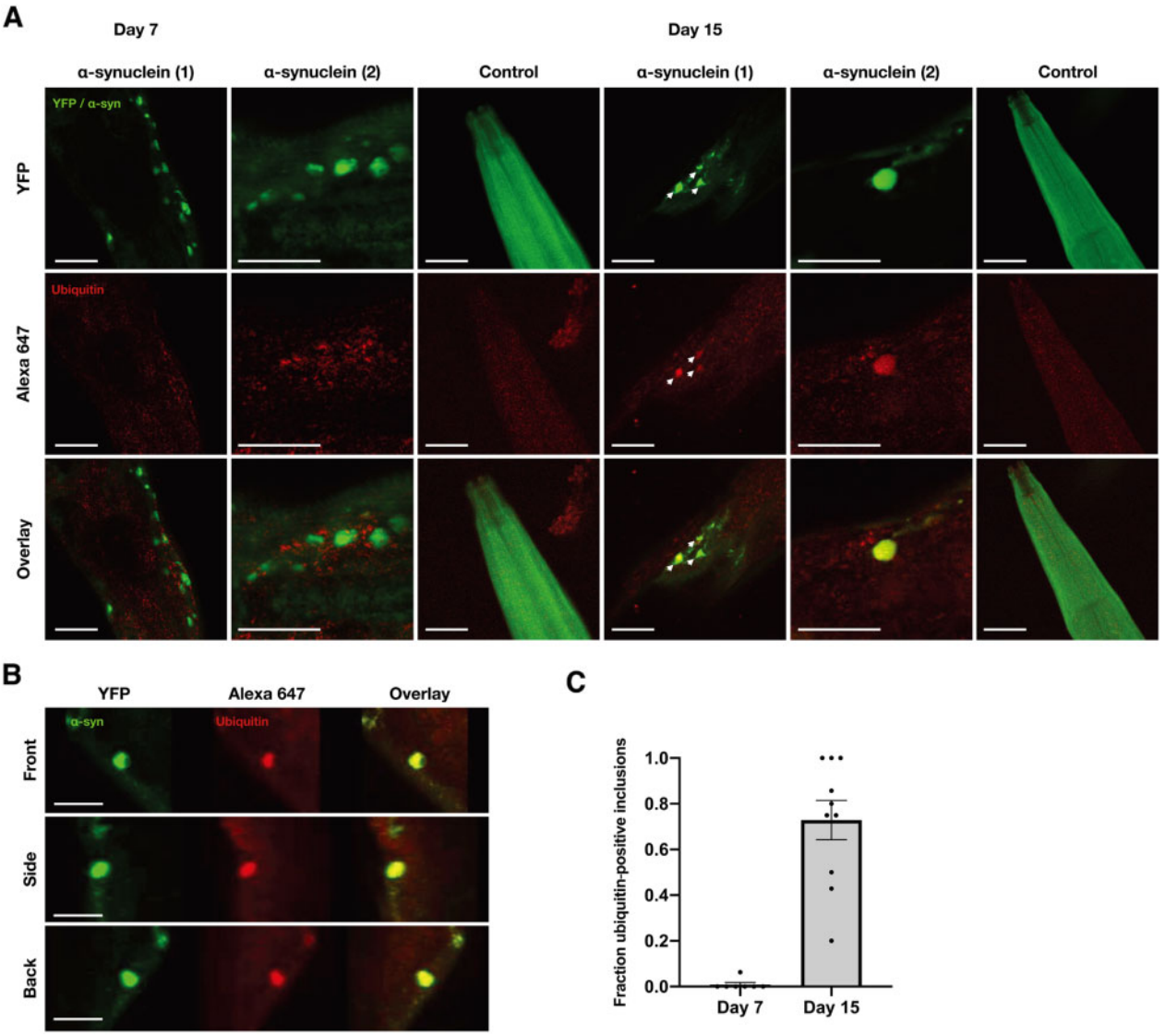

Figure 2 α-synuclein inclusions in aged worms are immunoreactive for ubiquitin. (**A**) Inclusions in aged worms (Day 15, right) are immunoreactive for ubiquitin, whereas inclusions in younger worms (Day 7, left) do not show immunoreactivity. For each time point, two representative animals are shown together with a control strain expressing only YFP. Scale bar, 20 μm. (**B**) 3D rendering of an image stack showing co-localization of α-synuclein–YFP and Alexa 647 anti-ubiquitin signal in an aged worm (Day 15). Scale bar, 10 μm. (**C**) Quantification of ubiquitin-positive inclusions at indicated time points. Each datapoint represents the average number of ubiquitin-positive inclusions in one worm. Results are mean ± SEM.

biophysical properties of α-synuclein, we tested its capability of forming such assemblies *in vitro*. We incubated Alexa 488-labelled human α-synuclein at physiological pH and in the presence of polyethylene glycol (PEG 12000), a commonly used crowding agent that does not affect the unfolded conformation of α-synuclein (Munishkina et al., 2004; Mcnulty et al., 2006; Materials and methods). When deposited on a glass surface, α-synuclein formed micron-sized droplets within several minutes (Figures 4A; Supplementary Movie S2), at concentrations that can be found at the pre-synaptic terminal (± 50–100 μM) as well as concentrations associated with pathological overexpression (>100 μM) (Supplementary Figure S3; Bodner et al., 2009; Wilhelm et al., 2014). Droplet formation was sensitive to ionic strength (Supplementary Figure S4), which is likely the result of the involvement of the acidic C-terminal region of α-synuclein. We predicted that this region can spontaneously phase-separate via disordered interactions (Supplementary Figure S5), which are likely involved in the stabilization of the droplet in conjunction with hydrophobic effects mediated by the NAC region (Hardenberg et al., 2020; Ray et al., 2020). To characterize whether α-synuclein droplets had properties of a liquid phase, we assessed two key biophysical features. First, we observed

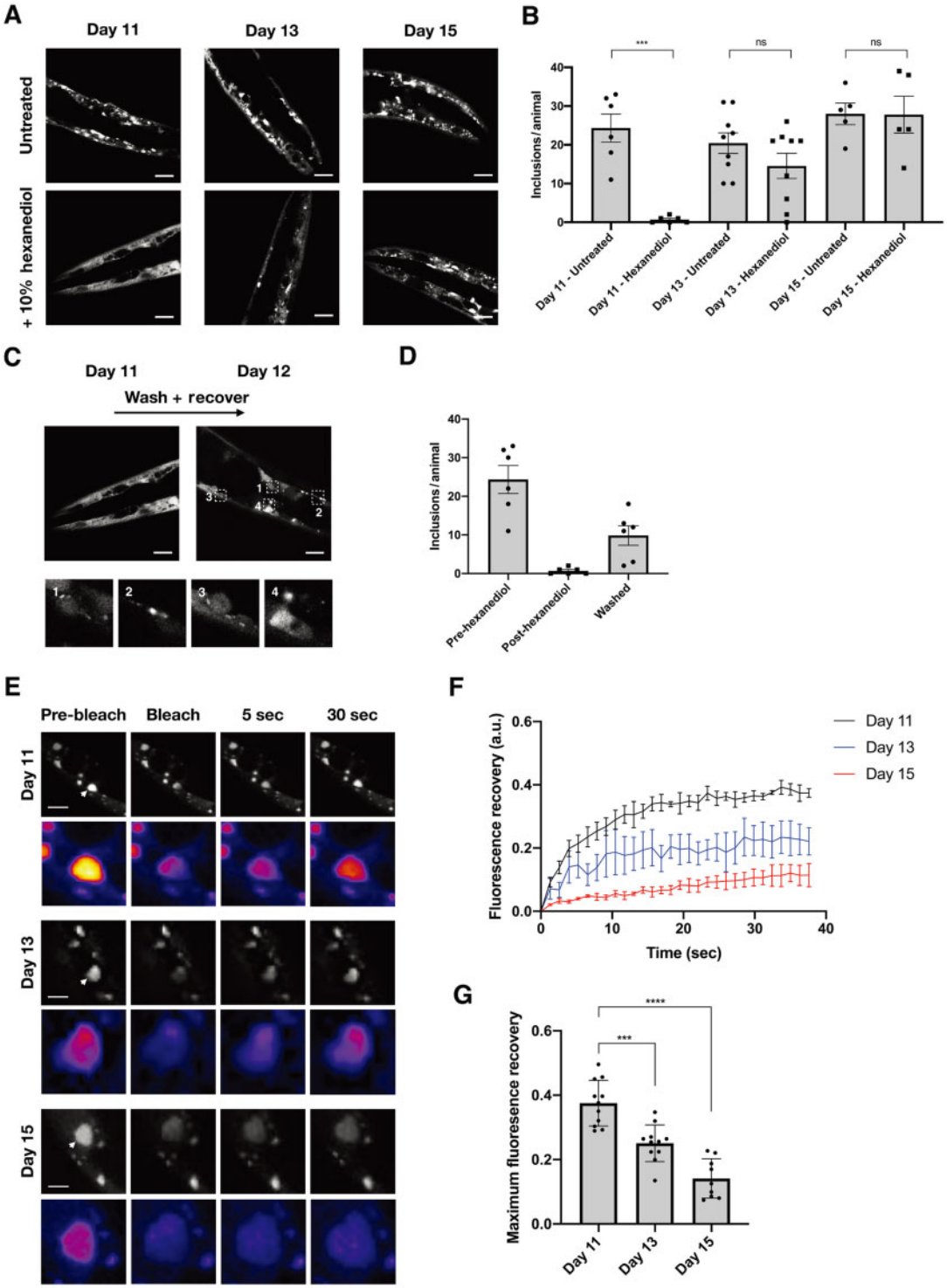

Figure 3 Early α-synuclein inclusions in *C. elegans* have liquid-like properties. (**A**) Exposure to 10% (*w*/*v*) 1,6-hexanediol dissolves α-synuclein inclusions in body wall muscle cells between Days 1 and 11 of adulthood, reflecting the dependence of inclusion assembly on weak hydrophobic interactions. By contrast, inclusions in aged nematodes (Days 13–15 of adulthood) appear to be amyloid-like, as evidenced by decreased hexanediol efficacy. (**B**) Quantification of images in **A**. Each square or circle represents one animal from the population. (**C**) α-synuclein assemblies in younger nematodes reappear after hexanediol is washed out. Newly formed small inclusions were observed in washed worms after one day of recovery, reflecting the dynamic and liquid-like nature of α-synuclein assemblies in *C. elegans*. (**D**) Quantification of images in **C**. Scale bar, 25 μm. (**E**) FRAP of α-synuclein inclusions at indicated time points. Scale bar, 10 μm. (**F**) Average recovery trace of all inclusions in a single worm at indicated time points. Error bars represent SEM. (**G**) Maximum fluorescent recovery at indicated time points. Each datapoint represents the average maximum recovery of all inclusions in a single worm. Results are mean ± SEM. One-way ANOVA; ***$P \leq 0.001$; ****$P \leq 0.0001$; ns, not significant.

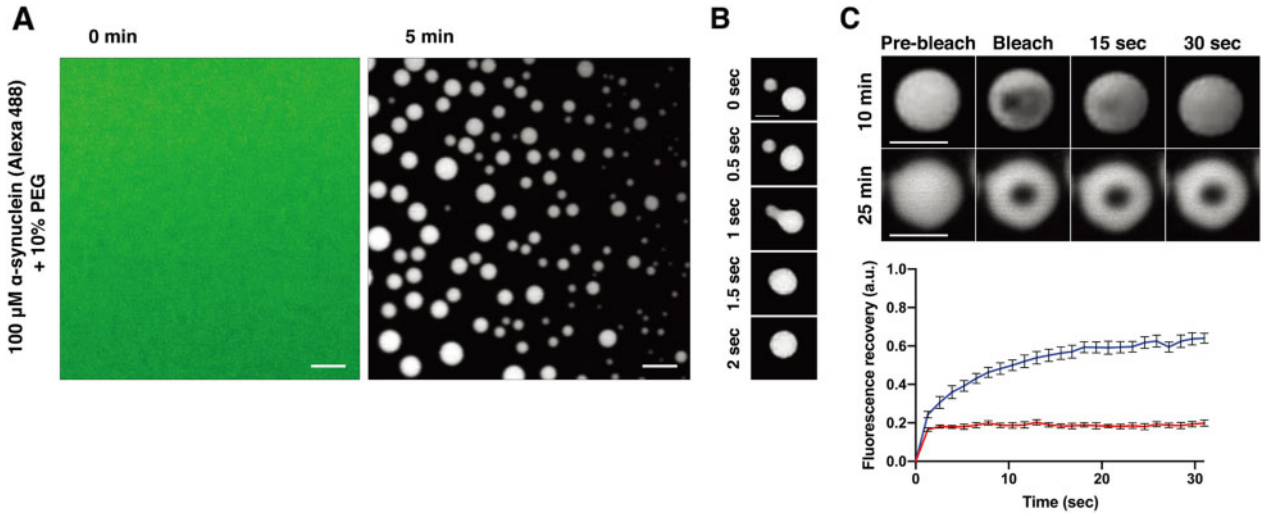

Figure 4 α-synuclein undergoes liquid–liquid phase separation *in vitro*. (**A**) Wild-type human α-synuclein (100 μM) in the presence of 10% PEG, supplemented with 1 mol% Alexa 488-labelled α-synuclein, forms micrometre-sized droplets under physiological conditions. Scale bar, 5 μm. (**B**) Fusion of two α-synuclein droplets in close proximity (<1 μm). Scale bar, 1 μm. (**C**) FRAP of a small area within the droplet. Red line represents aged droplets. Scale bar, 1 μm; error bars represent SEM.

that two droplets readily fuse and relax into a larger droplet once they come in close proximity (<1 μm) (Figure 4B; Supplementary Movie S3). Second, FRAP of a small area within the droplet was followed by rapid recovery ($t_{1/2}$ = 5 sec), reflecting local rearrangement of α-synuclein molecules within the condensate (Figure 4C; Supplementary Movie S4).

The conversion of α-synuclein droplets into gel-like assemblies is associated with amyloid formation

The ability of α-synuclein molecules to rearrange within droplets declines over time (Figure 4C), which is in line with the thermodynamic drive of dense protein solutions to mature into more solid-like states, such as highly ordered amyloid fibrils (Molliex et al., 2015; Patel et al., 2015; Harmon et al., 2017; Wegmann et al., 2018). To test whether the maturation of α-synuclein droplets is associated with amyloid formation, we assessed this process using turbidity measurements in the presence of the amyloid-binding dye thioflavin T (ThT) (Figure 5A and B). Droplet formation as seen from increased turbidity at 540 nm was followed by increased ThT fluorescence, indicating that droplet ageing involves the formation of amyloid species. Furthermore, a hydrogel with amyloid-like features could be recovered at the end of each incubation period (Figure 5C). These results indicate that under physiological conditions, α-synuclein can undergo a phase transition into a dynamic liquid droplet state, which converts into gel-like aggregates over time.

α-synuclein droplets age more slowly when merged with liposomes

In dopaminergic neurons, α-synuclein is highly concentrated at pre-synaptic terminals where it can transiently bind to a variety of lipid surfaces, including those of synaptic vesicles (Burré et al., 2010, 2014; Fusco et al., 2016; Lautenschläger et al., 2018). These observations lead to the question of whether synaptic vesicles modulate the phase behaviour of α-synuclein. We thus incubated α-synuclein with liposomes with a composition mimicking that of synaptic vesicles (Takamori et al., 2006; Materials and methods). To enable detection by fluorescence microscopy, liposomes were supplemented with a fluorescently labelled lipid, 1,2-dioleoyl-sn-glycero-3-phosphoethanolamine-N-(cyanine 5) (Cy5-DOPE) (Materials and methods). Formation of α-synuclein droplets coincided with the appearance of condensates that were positive for the labelled lipid (Figure 6A; Supplementary Movie S5), whereas liposomes alone either remained diffuse or formed irregular aggregates (Figure 6B). Co-localization of lipids and α-synuclein at droplets was dependent on the protein:lipid ratio (Figure 6A), where a higher ratio resulted in reduced mixing of liposomes and α-synuclein (Figure 6A, bottom). 3D rendering of the droplets showed that lipids are directly recruited into α-synuclein droplets (Figure 6C; Supplementary Movie S6), in which α-synuclein continues to behave as a liquid phase as evidenced by rapid fusion of two α-synuclein/lipid droplets (Figure 6D). Crucially, α-synuclein/lipid droplets appeared to be more resistant to ageing, as the protein in these mixed droplets showed a slower decline in FRAP when compared to pure α-synuclein droplets (Figure 6E). This effect was lost when the concentration of liposomes was reduced. We also note that the lipids inside the droplets have limited FRAP, suggesting that they are either restricted in their mobility or stabilized upon interaction with α-synuclein (Figure 6E, bottom). Taken together, these results suggest that liposomes mimicking synaptic vesicles stabilize the liquid state of α-synuclein, which could reflect the native environment of α-synuclein where synaptic membranes are highly abundant. Indeed, reduced aggregation in the presence

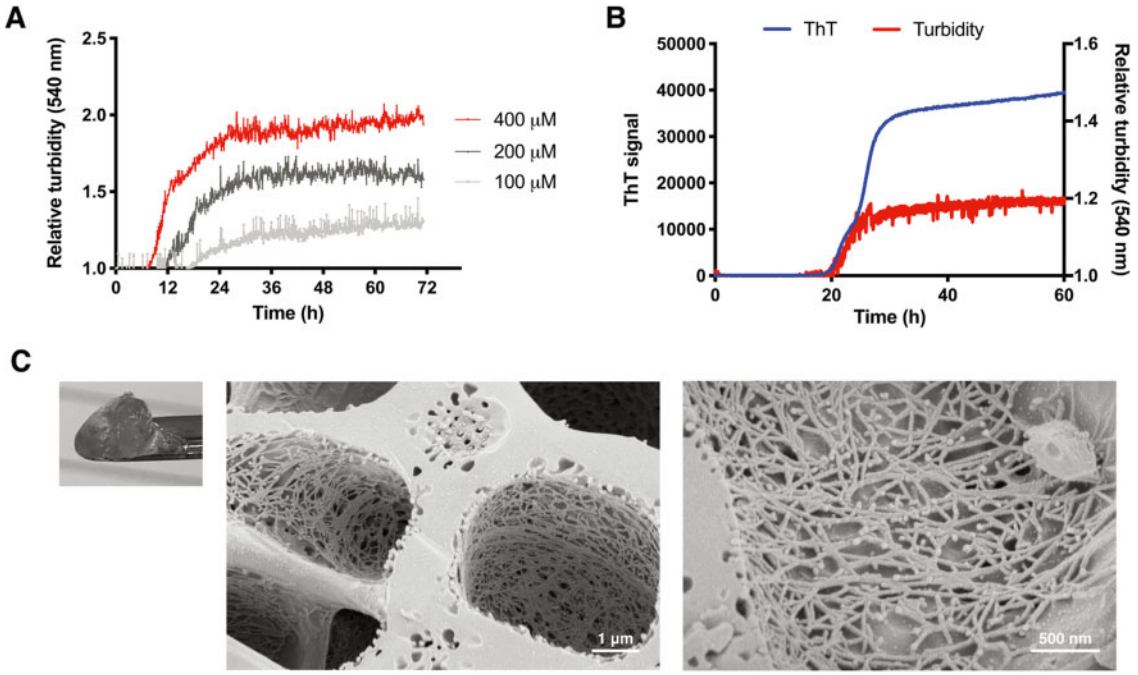

Figure 5 α-synuclein droplets mature into amyloid-like hydrogels *in vitro*. (**A**) α-synuclein in the presence of 10% PEG becomes turbid, representing the formation of light-scattering objects such as droplets. Datapoints represent 5-min-interval measurements, preceded by brief shaking. (**B**) α-synuclein becomes positive for ThT following an increase in turbidity, indicating that the assemblies adopt an amyloid-like nature. (**C**) Cryo-SEM image of α-synuclein hydrogel formed at the end of the experiment shown in **B**. Left panel shows the hydrogel. The morphology as seen by cryo-SEM (middle and right panels) indicates that hydrogels are rich in fibrillar structures. Scale bar, 1 μm (middle) and 500 nm (right).

of synaptic membranes is expected, as the binding of α-synuclein to these membranes does not readily trigger amyloid formation *in vitro* (Galvagnion et al., 2016). In this context, the binding of α-synuclein to the surface of liposomes likely reduces the amount of α-synuclein available to engage in β-sheet formation, consistent with the law of mass action. A converse effect can be observed for membranes with primarily charged headgroups, which have an overall aggregation promoting effect (Galvagnion et al., 2016), and have been shown to accelerate ageing of α-synuclein droplets (Ray et al., 2020).

Discussion

We have shown that α-synuclein forms liquid-like condensates *in vivo* in a *C. elegans* model of PD and *in vitro* at physiological concentrations and pH. Our FLIM analysis indicated that the inclusions formed by α-synuclein in *C. elegans* body wall muscle cells are largely non-amyloid and can be dissociated by 1,6-hexanediol. α-synuclein droplets behave as a liquid phase *in vitro*, as individual α-synuclein molecules rapidly rearrange within the droplets, and individual droplets were observed to fuse and relax back into a spherical shape.

These observations can be linked to the increasing evidence that the phenomenon of liquid–liquid phase separation underlies the organization of proteins at the synapse (Milovanovic et al., 2018; Chen et al., 2020). It has also been shown that α-synuclein clusters synaptic vesicles and regulates the synaptic vesicle pool (Burré et al., 2010; Bendor et al., 2013; Fusco et al., 2016; Lautenschläger et al., 2018). In this context, our results suggest that droplet formation by α-synuclein may be involved in a physiological mechanism to cluster synaptic vesicles, possibly in conjunction with other proteins such as synapsins, which have also been shown to phase-separate into liquid-like assemblies (Milovanovic et al., 2018). Indeed, synapsins are implicated in synaptic function in conjunction with synuclein (Zaltieri et al., 2015; Atias et al., 2019) and are components of Lewy bodies (Longhena et al., 2018).

We have also shown that the droplet state can undergo a maturation process into a gel-like state rich in amyloid structure and immunoreactive for ubiquitin, which is reminiscent of the pathological state seen in Lewy body pathologies (Spillantini et al., 1997, 1998; Araki et al., 2019). This phenomenon is expected on the grounds that the transition from the droplet state to the amyloid state takes place through a maturation process, known as Ostwald step rule (Boke et al., 2016; Yuan et al., 2019), and it is consistent with the recent report that α-synuclein can form hydrogels (Kumar et al., 2018; Pogostin et al., 2019). From a thermodynamic point of view, it is important to note that the gel-like assembly is not a stable state in addition to the native, the droplet and the amyloid states, but a slowly evolving conformation on pathway to the amyloid state (Figure 7A). This ageing process can become very slow depending on the complexity of the composition, and one can speculate that Lewy bodies are in a condition of nearly

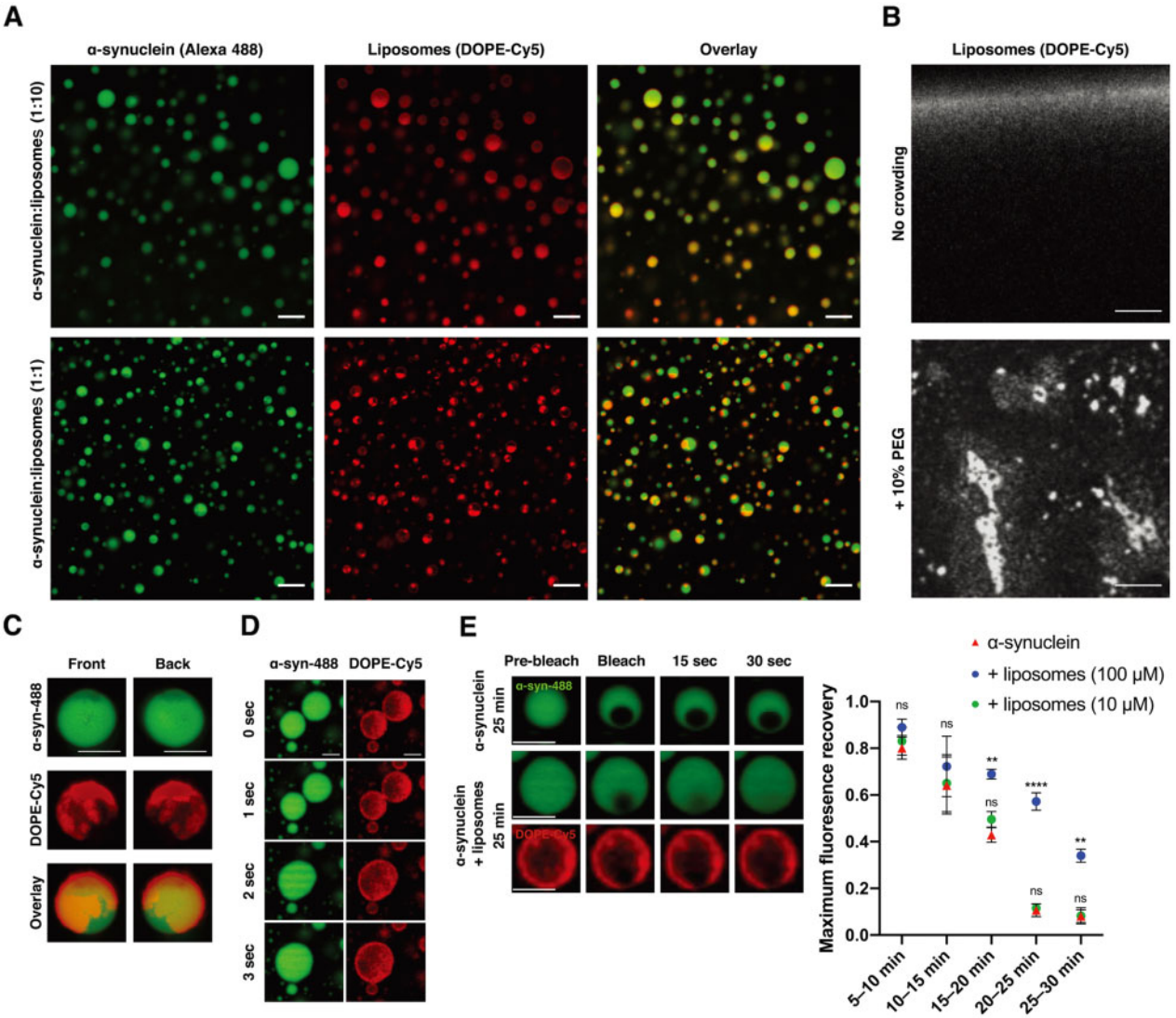

Figure 6 α-synuclein droplets co-localize with liposomes. (**A**) α-synuclein droplets co-localize with liposomes resembling the lipid composition of synaptic vesicles (DOPE:DOPC:DOPS) labelled with DOPE-Cy5. α-synuclein (100 μM) was incubated with either 1 mM (protein:lipid ratio at 1:10, top) or 100 μM liposomes (protein:lipid ratio at 1:1, bottom). Scale bar, 5 μm. (**B**) Liposomes (1 mM) in buffer remain diffuse (top) or form aggregates (bottom). Scale bar, 10 μm. (**C**) 3D rendering of the droplets showing that lipids are directly recruited into α-synuclein droplets (protein:lipid, 1:1). Scale bar, 1 μm. (**D**) Fusion of two α-synuclein/liposome droplets in close proximity (protein:lipid, 1:1). Scale bar, 1 μm. (**E**) α-synuclein/liposome droplets mature slower than droplets containing only α-synuclein (protein:lipid, 1:1). Lowering the protein:lipid ratio to 10:1 results in a loss of the protective effect. Each datapoint represents the average recovery of three droplets for that timeframe. Scale bar, 1 μm; error bars represent SEM. One-way ANOVA; $^{**}P \leq 0.01$; $^{****}P \leq 0.0001$; ns, not significant.

arrested maturation. In this context, we found that the sequestration of liposomes mimicking synaptic vesicles slows the maturation process, which is consistent with the observation that various lipid vesicles and membranes are found in Lewy bodies (Shahmoradian et al., 2019; Mahul-Mellier et al., 2020). We can thus suggest that the effects of such membranous structures on the ageing process of the droplets involve a slowing down of the amyloid conversion of the gel-like α-synuclein assemblies. This process could create a metastable toxic state, as gel-like assemblies are a reservoir for cytotoxic α-synuclein oligomers (Kumar et al., 2018).

We also note that the conversion of α-synuclein between the native state and the amyloid state can take place directly through a 'deposition pathway' (Figure 7B) following a more conventional nucleation–growth process (Buell et al., 2014), where the nucleation step can be catalysed by the presence of charged lipid membranes (Galvagnion et al., 2015), rather than the 'condensation pathway' described here (Figure 7B). Whether α-synuclein primarily follows the deposition route to the amyloid state or the condensation route through the droplet state is likely determined by the environmental conditions. One such condition could involve the lipid composition of

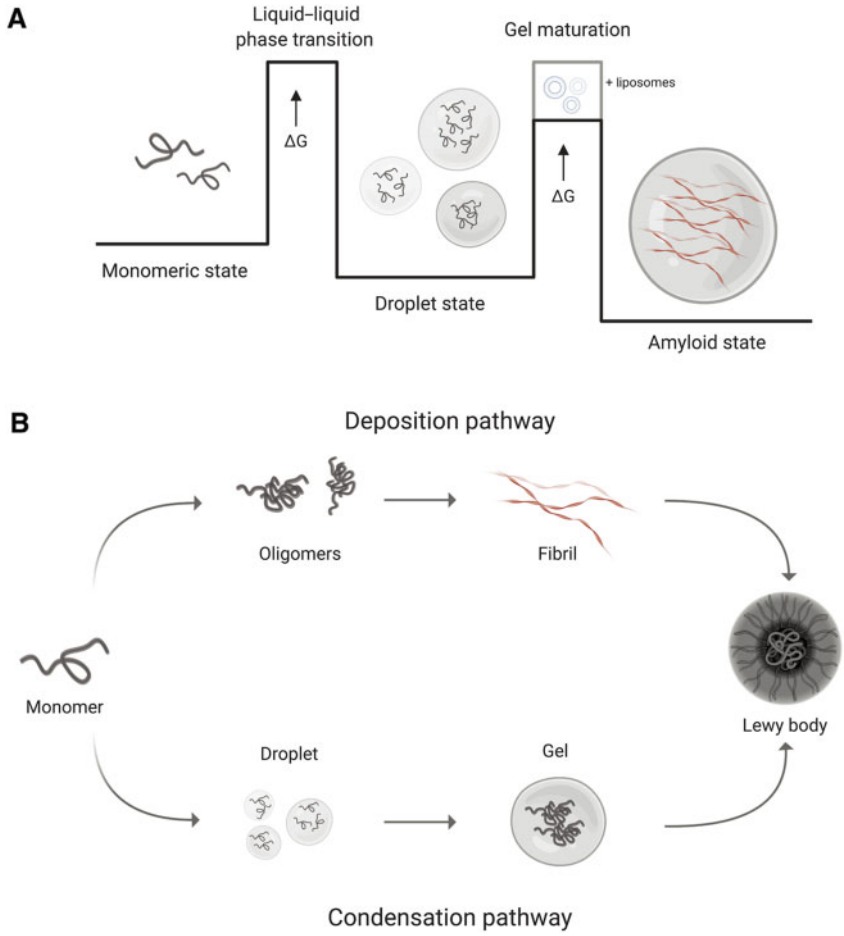

Figure 7 Schematic illustration of the possible deposition and condensation pathways of α-synuclein self-assembly into Lewy bodies. (**A**) α-synuclein can populate the monomeric state, the droplet state, and the amyloid state. The amyloid state is likely to be the thermodynamically most stable state under cellular conditions, but its kinetic accessibility is reduced by the presence of free energy barriers between the native and droplet states and between the droplet and amyloid states. The latter free energy barrier can be crossed through a maturation process that involves the formation of gel-like amyloid-rich assemblies that gradually age into the amyloid state. This slow conversion can become altogether arrested in the presence of cellular components, possibly resulting in the formation of Lewy bodies. (**B**) The conversion of α-synuclein from the monomeric to the amyloid state can proceed through two distinct pathways. In the 'deposition pathway', α-synuclein forms initially small disordered oligomers that then convert into ordered oligomers, which then grow into amyloid fibrils. In the 'condensation pathway', α-synuclein forms first a droplet state, which then gradually matures into the amyloid state going through gel intermediates. Although both pathways can be homogeneous, with α-synuclein as the sole component of the system, in complex environments, they are most likely heterogeneous, with other cellular components taking part in the process, including in particular lipid membranes.

membranes, since this determines the rate of α-synuclein nucleation, with membranes mimicking synaptic vesicles being unable to drive nucleation (Galvagnion et al., 2016). A decline in synaptic vesicle density, as observed for some PD mutations through altered synaptic protein function (Nguyen and Krainc, 2018), could therefore shift α-synuclein membrane binding with adverse consequences.

In conclusion, we have shown that α-synuclein undergoes liquid–liquid phase separation to adopt a droplet state and that this process may lead to the formation of aberrant gel-like assemblies with features of Lewy bodies.

Materials and methods

C. elegans strains and maintenance

Standard conditions were used for the propagation of *C. elegans* (Goldstein, 2016). We used the OW40 (zgIs15[unc-54p::α-synuclein::YFP] IV) strain in which α-synuclein is fused to YFP and stably expressed in body wall muscle cells (Van Ham et al., 2008). OW40 animals were synchronized by hypochlorite bleaching, hatched overnight in M9 buffer (3 g/L KH_2PO_4, 6 g/L Na_2HPO_4, 5 g/L NaCl, and 1 mM $MgSO_4$), and subsequently cultured at 20°C on nematode growth medium (NGM; 1 mM $CaCl_2$, 1 mM $MgSO_4$, 5 μg/ml cholesterol, 250 mM KH_2PO_4 [pH 6],

17 g/L agar, 3 g/L NaCl, and 7.5 g/L casein) plates, which were seeded with the *Escherichia coli* strain OP50. At L4 stage, larvae were placed on NGM plates containing 75 μM 5-fluoro-2′deoxyuridine (FUDR, Sigma) to inhibit the growth of offspring.

Estimation of C. elegans α-synuclein concentration

To estimate the concentration of α-synuclein at the *C. elegans* body wall muscle cells, 50 worms were hand-picked into 1× Laemmli buffer and heated at 100°C for 5 min. Simultaneously, known concentrations of purified human α-synuclein (see below '*α-synuclein purification and labelling*') were diluted in 1× Laemmli buffer and heated at 100°C for 5 min. Resulting protein solutions were then separated on a NuPAGE Novex 4%–12% Bis-Tris Protein Gels (Life Technologies) and transferred to nitrocellulose membranes using an iBlot Dry Blotting System (Life Technologies). To improve α-synuclein immunodetection, the membrane was treated with phosphate-buffered saline (PBS) containing 0.4% paraformaldehyde for 30 min at room temperature, followed by blocking for 1 h with 5% skim milk in PBS. Membranes were probed with the LB509 anti-α-synuclein antibody (1:1000; Abcam) overnight at 4°C and visualized with a fluorescent secondary antibody, Alexa 488-conjugated goat-anti-mouse IgG (1:5000, A11029, Life Technologies). Fluorescent bands were detected on a Typhoon FLA 7000 (GE Life Sciences) imaging system and quantified in ImageJ (National Institutes of Health). To determine the protein content per cell, α-synuclein levels were compared to the purified α-synuclein standard and the resulting value was divided by the number of cells in which the protein is expressed under the unc-54 promoter (95 body wall muscle cells, eight vulval muscle cells, and anal depressor cell). Finally, the volume of each cell used to calculate the final concentration was ±1 pl, as previously determined (Sinnige et al., 2020).

FLIM

At indicated time points, transgenic worms were washed off NGM plates in M9 buffer and mounted on 2.5% agarose pads on glass microscopy slides and immobilised using 10 mM levamisole hydrochloride (Merck). Slides were then mounted onto a modified, confocal-based platform (Olympus FV300-IX700) integrated with a time-correlated single photon counting module (SPC-830, B&H). Images of the anterior region of the worm were acquired at 60× (PLAPON 60×OSC2, 1.4NA, Olympus) magnification. For excitation of YFP, the output of a pulsed supercontinuum source (WL-SC-400-15, Fianium Ltd.) operating at 40 MHz repetition rate and filtered using a FF03-510/20 (Semrock Inc.) bandpass filter was used. YFP fluorescence emission was filtered with a FF01-542/27 (Semrock Inc.) bandpass filter. Photons were acquired for 2 min to create a single 256 × 256 image with 256 time bins. Inclusions were detected using a custom-designed image-processing pipeline in ImageJ. Briefly, cytoplasmic background was reduced through application of a Gaussian convolution filter and binarized according to the Chow and Kaneko adaptive thresholding method (Chow and Kaneko, 1972). Subsequently, clustered inclusions were separated using a classic watershed segmentation algorithm. The resulting image was then used to create a mask of the signal representing inclusions and subtracted from the total signal, creating a separate mask for the diffuse signal. Lifetime analysis of the processed images was carried out using FLIMFit (Imperial College London Photonics). FLIM data were fitted with a single exponential decay function to extract the fluorescence lifetime in each pixel using FLIMFit v4.12 (Warren et al., 2013).

Proteinase K assay

For proteinase K digestion assays, worms were lysed using a Balch homogenizer in NP-40 lysis buffer (150 mM NaCl, 1.0% NP-40, and 50 mM Tris, pH 8.0), as described previously (Bhaskaran et al., 2011). Lysates were kept on ice before being exposed to increasing proteinase K concentrations (0, 1, 2, and 3 μg/ml) for 30 min at 37°C. Following digestion, samples were immediately heated at 100°C for 5 min in Laemmli buffer, separated on NuPAGE Novex 4%–12% Bis-Tris Protein Gels, and subjected to immunoblotting for α-synuclein levels, as described above.

Ubiquitin antibody staining

For ubiquitin antibody staining in *C. elegans*, animals were washed off NGM plates in M9 buffer and transferred to Eppendorf tubes. Worms were fixed in three consecutive steps to prevent disturbing the liquid-like inclusions, while also maintaining structure and epitope availability; worms were first briefly exposed to ice-cold methanol (5 min, on ice), followed by ice-cold acetone (5 min, on ice), before incubation with 4% paraformaldehyde (20 min, at room temperature) (Thermo Fisher Pierce). Worms were washed with PBS between each fixation step, avoiding the use of centrifugation by letting the worms sediment on the bottom of the tube. Following fixation, animals were incubated with 1 ml of Alexa Fluor 647-conjugated anti-ubiquitin antibody (1:200, Abcam) for 1 h at room temperature. Excess antibody was removed by three PBS washes as described above, after which animals were embedded in 50 μl of thermo-reversible hydrogel (CyGEL™, Biostatus) and imaged on a Leica TCS SP8 inverted confocal microscope using a 40×/1.3 HC PL Apo CS oil objective (Leica Microsystems). Sequential line scanning was used to avoid bleed through of the YFP signal.

Hexanediol experiments

To achieve slow diffusion of 1,6-hexanediol into the worms without eliciting rapid toxic effects, animals were washed off NGM plates in M9 buffer and embedded in 20 μl of thermo-reversible hydrogel (CyGEL™, Biostatus) supplemented with 10% (*w*/*v*) 1,6-hexanediol (Sigma) and 10 mM levamisole hydrochloride (Merck) on a glass-bottom imaging dish (MatTek P35G-1.5-14-C). For control experiments, worms were embedded in hydrogel with 10% dH_2O and 10 mM levamisole hydrochloride. Glass-bottom dishes were subsequently sealed with a

12 mm × 12 mm 1.5 cover glass (Fisherbrand) and left at room temperature for 1 h. After incubation, worms were imaged on a Leica SP8 upright confocal microscope using a 40×/1.3 HC PL Apo CS oil objective (Leica Microsystems). For recovery experiments, imaging dishes were cooled on ice until the hydrogel liquified and immediately diluted in M9 buffer. Worms were then washed twice in M9 buffer, before being left to recover on seeded NGM plates for 24 h. Hereafter, worms were imaged as described above.

α-synuclein purification and labelling

Wild-type and A90C α-synuclein were purified from *E. coli* expressing plasmid pT7-7 encoding the protein as previously described (Hoyer et al., 2002; Cremades et al., 2012). Following purification, the protein was concentrated using Amicon Ultra-15 Centrifugal Filter Units (Merck Millipore). A90C α-synuclein was labelled with 1.5-fold molar excess Alexa Fluor 488 C_5 maleimide (Life Technologies) overnight at 4°C. The excess dye was removed on a Sephadex G-25 desalting column (Sigma) as described previously (Cremades et al., 2012), and the buffer was exchanged into 25 mM Tris-HCl (pH 7.4).

Liquid–liquid phase separation assay

To induce droplet formation, non-labelled wild-type α-synuclein was mixed with Alexa Fluor 488-labelled A90C α-synuclein at a 10:1 molar ratio in 25 mM Tris-HCl (pH 7.4), 50 mM NaCl, 1 mM DTT, and 10% PEG 12000 (Thermo Fisher Scientific) at 20°C, unless indicated otherwise. The final mixture was pipetted onto a 35-mm glass-bottom dish (P35G-1.5-20-C, MatTek Life Sciences) and immediately imaged on a Leica TCS SP5 confocal microscope using a 40×/1.3 HC PL Apo CS oil objective (Leica Microsystems). The excitation wavelength was 488 nM for all experiments. All images were processed and analysed in ImageJ.

FRAP

FRAP was performed on the setup described above for the liquid–liquid phase separation assay, under the same experimental conditions. Bleaching was done using the 488 nm laser at 50% intensity, to obtain ±50%–60% relative photobleaching. Images were captured at 600 ms intervals, following a 1.8-sec (3-frame) pre-bleach sequence and a 1.2-sec (2-frame) spot bleach covering 30%–50% of the droplet area. Intensity traces of the bleached area were background corrected and normalized.

For *C. elegans* experiments, worms were immobilized in 20 µl CyGEL™ (Biostatus) supplemented with 10 mM levamisole hydrochloride and placed on a glass-bottom imaging dish (MatTek P35G-1.5-14-C).

Liposome preparation

Small unilamellar vesicles were prepared to approximate the lipid composition of synaptic vesicles (Takamori et al., 2006), 50 mol% DOPC (1,2-dioleoyl-sn-glycero-3-phosphocholine), 30 mol% DOPE (1,2-dioleoyl-sn-glycero-3-phosphatidylethanolamine), and 20 mol% DOPS (1,2-dioleoyl-sn-glycero-3-phospho-L-serine), supplemented with 1 mol% DOPE-Cy5 (Avanti Polar Lipids). Lipids were mixed in chloroform and dried under a mild stream of nitrogen gas. Dried lipids were then lyophilized for 3 h (VWR, Avantor), before being rehydrated in 25 mM Tris-HCl (pH 7.4). Liposomes were formed by 10 consecutive freeze–thaw cycles (–196°C to 30°C). To form uniformly sized liposomes, the mixture was extruded 20 times through 50 nm-diameter polycarbonate filters (Avanti Polar Lipids). Liposome size distribution was confirmed using dynamic light scattering (average size ±50 nm) and re-extruded when standard deviation >20 nm.

Turbidity and ThT assay

Wild-type α-synuclein was mixed with 20 µM ThT in 25 mM Tris-HCl (pH 7.4), 50 mM NaCl, and 10% PEG 12000 at 2°C. All samples were prepared in low binding test tubes (Eppendorf), after which each sample was pipetted in triplicate into a 96-well half-area, low-binding, clear-bottom plate (Corning) on ice. Assays were initiated by placing the 96-well plate at 20°C under intermediate (5 min) shaking (100 rpm, 10 sec) conditions in a plate reader (Fluostar Omega or Fluostar Optima, BMG Labtech). The absorbance at 540 nm was measured every 5 min over 72 h. ThT fluorescence was measured through the bottom of the plate with a 440-nm excitation filter and a 480-nm emission filter.

Scanning electron microscopy (cryo-SEM)

Cryo-SEM was performed on a Verios 460 scanning electron microscope (FEI/Thermo Fisher) equipped with a Quorum PP3010T cryo-transfer system. Hydrogel samples were pipetted into shuttle-mounted universal cryo-stubs and flash-frozen in slushed nitrogen. After transfer into the prep-chamber, samples were fractured, sublimed at −90°C for 2 min, sputter-coated with a thin layer of platinum, and transferred to the SEM cryo-stage. Both prep-chamber and cryo-stage were set to −140°C. SE-imaging was performed at 1 keV accelerating voltage and 25 pA probe current using the Through-Lens-Detector (TLD) in immersion mode. Images were acquired with a pixel resolution of 1536 × 1024 pixels using a 300-ns dwell time/32 image integrations and using drift correction.

Droplet predictions

The binding modes of α-synuclein, as the probability to undergo disorder-to-order (P_{DO}) or disorder-to-disorder (P_{DD}) transitions upon interactions, were predicted from the amino acid sequence using the FuzPred program (protdyn-fuzpred.org) (Miskei et al., 2020). The FuzPred-Droplet method was used to estimate the probability for spontaneous liquid–liquid phase separation based on disorder in the free and bound states (Hardenberg et al., 2020).

Statistical analysis

All statistical analysis was performed in GraphPad Prism 8 (GraphPad Software). Data are presented as mean ± SEM from

at least three independent biological replicates, unless indicated otherwise. Statistical significance between experimental groups was analysed either by two-tailed Student's *t*-test or one-way ANOVA followed by Bonferroni's multiple comparison.

Supplementary material

Supplementary material is available at *Journal of Molecular Cell Biology* online.

Acknowledgements

We would like to acknowledge Nicola Lawrence at the Gurdon Institute Imaging Facility for confocal microscopy support and Karen Müller at the Cambridge Advanced Imaging Centre for her assistance with cryo-SEM experiments. We wish to thank Swapan Preet for her assistance with the protein purification and Wing Man for his help with the preparation of liposomes.

Funding

G.S.K.S. acknowledges funding from the Wellcome Trust (065807/Z/01/Z and 203249/Z/16/Z), the UK Medical Research Council (MRC; MR/K02292X/1), Alzheimer Research UK (ARUK; ARUK-PG013-14), Michael J Fox Foundation (16238), and from Infinitus China Ltd. S.T.D. acknowledges funding from the Biotechnology and Biological Sciences Research Council (BBSRC; BB/M011194/1).

Conflict of interest: none declared.

References

Ader, C., Frey, S., Maas, W., et al. (2010). Amyloid-like interactions within nucleoporin FG hydrogels. Proc. Natl Acad. Sci. USA *107*, 6281–6285.

Ambadipudi, S., Biernat, J., Riedel, D., et al. (2017). Liquid–liquid phase separation of the microtubule-binding repeats of the Alzheimer-related protein Tau. Nat. Commun. *8*, 275.

Araki, K., Yagi, N., Aoyama, K., et al. (2019). Parkinson's disease is a type of amyloidosis featuring accumulation of amyloid fibrils of α-synuclein. Proc. Natl Acad. Sci. USA *116*, 17963–17969.

Arima, K., Uéda, K., Sunohara, N., et al. (1998). Immunoelectron-microscopic demonstration of NACP/α-synuclein-epitopes on the filamentous component of Lewy bodies in Parkinson's disease and in dementia with Lewy bodies. Brain Res. *808*, 93–100.

Atias, M., Tevet, Y., Sun, J., et al. (2019). Synapsins regulate α-synuclein functions. Proc. Natl Acad. Sci. USA *116*, 11116–11118.

Banani, S.F., Lee, H.O., Hyman, A.A., et al. (2017). Biomolecular condensates: organizers of cellular biochemistry. Nat. Rev. Mol. Cell Biol. *18*, 285–298.

Bendor, J.T., Logan, T.P., and Edwards, R.H. (2013). The function of α-synuclein. Neuron *79*, 1044–1066.

Bhaskaran, S., Butler, J.A., Becerra, S., et al. (2011). Breaking *Caenorhabditis elegans* the easy way using the Balch homogenizer: an old tool for a new application. Anal. Biochem. *413*, 123–132.

Bodner, C.R., Dobson, C.M., and Bax, A. (2009). Multiple tight phospholipid-binding modes of α-synuclein revealed by solution NMR spectroscopy. J. Mol. Biol. *390*, 775–790.

Boeynaems, S., Alberti, S., Fawzi, N.L., et al. (2018). Protein phase separation: a new phase in cell biology. Trends Cell Biol. *28*, 420–435.

Boke, E., Ruer, M., Wühr, M., et al. (2016). Amyloid-like self-assembly of a cellular compartment. Cell *166*, 637–650.

Brundin, P., Dave, K.D., and Kordower, J.H. (2017). Therapeutic approaches to target α-synuclein pathology. Exp. Neurol. *298*, 225–235.

Buell, A.K., Galvagnion, C., Gaspar, R., et al. (2014). Solution conditions determine the relative importance of nucleation and growth processes in α-synuclein aggregation. Proc. Natl Acad. Sci. USA *111*, 7671–7676.

Burré, J., Sharma, M., and Südhof, T.C. (2014). α-synuclein assembles into higher-order multimers upon membrane binding to promote SNARE complex formation. Proc. Natl Acad. Sci. USA *111*, E4274–E4283.

Burré, J., Sharma, M., Tsetsenis, T., et al. (2010). α-synuclein promotes SNARE-complex assembly in vivo and in vitro. Science *329*, 1663–1667.

Chen, X., Wu, X., Wu, H., et al. (2020). Phase separation at the synapse. Nat. Neurosci. *23*, 301–310.

Chow, C., and Kaneko, T. (1972). Automatic boundary detection of the left ventricle from cineangiograms. Comput. Biomed. Res. *5*, 388–410.

Cohen, S.I.A., Vendruscolo, M., Dobson, C.M., et al. (2011). Nucleated polymerization with secondary pathways. II. Determination of self-consistent solutions to growth processes described by non-linear master equations. J. Chem. Phys. *135*, 065106.

Cremades, N., Cohen, S.I., Deas, E., et al. (2012). Direct observation of the interconversion of normal and toxic forms of α-synuclein. Cell *149*, 1048–1059.

Davis, A.A. (2020). Beyond synuclein: organelle accumulation in Lewy bodies may drive neurodegeneration. Sci. Transl. Med. *12*, eabb2778.

Dawson, T.M., and Dawson, V.L. (2003). Molecular pathways of neurodegeneration in Parkinson's disease. Science *302*, 819–822.

Dehay, B., Bourdenx, M., Gorry, P., et al. (2015). Targeting α-synuclein for treatment of Parkinson's disease: mechanistic and therapeutic considerations. Lancet Neurol. *14*, 855–866.

Fusco, G., Pape, T., Stephens, A.D., et al. (2016). Structural basis of synaptic vesicle assembly promoted by α-synuclein. Nat. Commun. *7*, 12563.

Galvagnion, C., Brown, J.W., Ouberai, M.M., et al. (2016). Chemical properties of lipids strongly affect the kinetics of the membrane-induced aggregation of α-synuclein. Proc. Natl Acad. Sci. USA *113*, 7065–7070.

Galvagnion, C., Buell, A.K., Meisl, G., et al. (2015). Lipid vesicles trigger α-synuclein aggregation by stimulating primary nucleation. Nat. Chem. Biol. *11*, 229.

Goedert, M., Jakes, R., and Spillantini, M.G. (2017). The synucleinopathies: twenty years on. J. Parkinson's Dis. *7*, S51–S69.

Goldstein, B. (2016). Sydney Brenner on the genetics of Caenorhabditis elegans. Genetics *204*, 1.

Hardenberg, M., Horvath, A., Ambrus, V., et al. (2020). Widespread occurrence of the droplet state of proteins in the human proteome. Proc. Natl Acad. Sci. USA *117*, 33254–33262.

Harmon, T.S., Holehouse, A.S., Rosen, M.K., et al. (2017). Intrinsically disordered linkers determine the interplay between phase separation and gelation in multivalent proteins. eLife *6*, e30294.

Hoyer, W., Antony, T., Cherny, D., et al. (2002). Dependence of α-synuclein aggregate morphology on solution conditions. J. Mol. Biol. *322*, 383–393.

Hyman, A.A., Weber, C.A., and Jülicher, F. (2014). Liquid–liquid phase separation in biology. Annu. Rev. Cell Dev. Biol. *30*, 39–58.

Iljina, M., Garcia, G.A., Horrocks, M.H., et al. (2016). Kinetic model of the aggregation of α-synuclein provides insights into prion-like spreading. Proc. Natl Acad. Sci. USA *113*, E1206–E1215.

Kaminski Schierle, G.S., Bertoncini, C.W., Chan, F.T., et al. (2011). A FRET sensor for non-invasive imaging of amyloid formation in vivo. ChemPhysChem *12*, 673–680.

Kanaan, N.M., Hamel, C., Grabinski, T., et al. (2020). Liquid–liquid phase separation induces pathogenic tau conformations in vitro. Nat. Commun. *11*, 2809.

Knowles, T.P.J., Waudby, C.A., Devlin, G.L., et al. (2009). An analytical solution to the kinetics of breakable filament assembly. Science *326*, 1533–1537.

Ko, L.W., Ko, H.H., Lin, W.L., et al. (2008). Aggregates assembled from overexpression of wild-type α-synuclein are not toxic to human neuronal cells. J. Neuropathol. Exp. Neurol. *67*, 1084–1096.

Kroschwald, S., Maharana, S., and Simon, A. (2017). Hexanediol: a chemical probe to investigate the material properties of membrane-less compartments. Matters *3*, e201702000010.

Kumar, R., Das, S., Mohite, G.M., et al. (2018). Cytotoxic oligomers and fibrils trapped in a gel-like state of α-synuclein assemblies. Angew. Chem. Int. Ed. *57*, 5262–5266.

Laine, R.F., Sinnige, T., Ma, K.Y., et al. (2019). Fast fluorescence lifetime imaging reveals the aggregation processes of α-synuclein and polyglutamine in aging Caenorhabditis elegans. ACS Chem. Biol. *14*, 1628–1636.

Lautenschläger, J., Stephens, A.D., Fusco, G., et al. (2018). C-terminal calcium binding of α-synuclein modulates synaptic vesicle interaction. Nat. Commun. *9*, 712.

Li, B., Ge, P., Murray, K.A., et al. (2018). Cryo-EM of full-length α-synuclein reveals fibril polymorphs with a common structural kernel. Nat. Commun. *9*, 3609.

Longhena, F., Faustini, G., Varanita, T., et al. (2018). Synapsin III is a key component of α-synuclein fibrils in Lewy bodies of PD brains. Brain Pathol. *28*, 875–888.

Mahul-Mellier, A.-L., Burtscher, J., Maharjan, N., et al. (2020). The process of Lewy body formation, rather than simply α-synuclein fibrillization, is one of the major drivers of neurodegeneration. Proc. Natl Acad. Sci. USA *117*, 4971–4982.

Mcnulty, B.C., Young, G.B., and Pielak, G.J. (2006). Macromolecular crowding in the Escherichia coli periplasm maintains α-synuclein disorder. J. Mol. Biol. *355*, 893–897.

Milovanovic, D., Wu, Y., Bian, X., et al. (2018). A liquid phase of synapsin and lipid vesicles. Science *361*, 604–607.

Miskei, M., Horváth, A., Vendruscolo, M., et al. (2020). Sequence-based determinants and prediction of fuzzy interactions in protein complexes. J. Mol. Biol. *432*, 2289–2303.

Molliex, A., Temirov, J., Lee, J., et al. (2015). Phase separation by low complexity domains promotes stress granule assembly and drives pathological fibrillization. Cell *163*, 123–133.

Munishkina, L.A., Cooper, E.M., Uversky, V.N., et al. (2004). The effect of macromolecular crowding on protein aggregation and amyloid fibril formation. J. Mol. Recognit. *17*, 456–464.

Murakami, T., Qamar, S., Lin, J.Q., et al. (2015). ALS/FTD mutation-induced phase transition of FUS liquid droplets and reversible hydrogels into irreversible hydrogels impairs RNP granule function. Neuron *88*, 678–690.

Nguyen, M., and Krainc, D. (2018). LRRK2 phosphorylation of auxilin mediates synaptic defects in dopaminergic neurons from patients with Parkinson's disease. Proc. Natl Acad. Sci. USA *115*, 5576–5581.

Patel, A., Lee, H.O., Jawerth, L., et al. (2015). A liquid-to-solid phase transition of the ALS protein FUS accelerated by disease mutation. Cell *162*, 1066–1077.

Poewe, W., Seppi, K., Tanner, C.M., et al. (2017). Parkinson disease. Nat. Rev. Dis. Primers *3*, 17013.

Pogostin, B.H., Linse, S., and Olsson, U. (2019). Fibril charge affects α-synuclein hydrogel rheological properties. Langmuir *35*, 16536–16544.

Polymeropoulos, M.H., Lavedan, C., Leroy, E., et al. (1997). Mutation in the α-synuclein gene identified in families with Parkinson's disease. Science *276*, 2045–2047.

Poudel, C., Mela, I., and Kaminski, C.F. (2020). High-throughput, multi-parametric, and correlative fluorescence lifetime imaging. Methods Appl. Fluoresc. *8*, 024005.

Ray, S., Singh, N., Kumar, R., et al. (2020). α-synuclein aggregation nucleates through liquid–liquid phase separation. Nat. Chem. *12*, 705–716.

Schapira, A.H., Olanow, C.W., Greenamyre, J.T., et al. (2014). Slowing of neurodegeneration in Parkinson's disease and Huntington's disease: future therapeutic perspectives. Lancet *384*, 545–555.

Schweighauser, M., Shi, Y., Tarutani, A., et al. (2020). Structures of α-synuclein filaments from multiple system atrophy. Nature *585*, 464–469.

Shahmoradian, S.H., Lewis, A.J., Genoud, C., et al. (2019). Lewy pathology in Parkinson's disease consists of crowded organelles and lipid membranes. Nat. Neurosci. *22*, 1099–1109.

Shin, Y., and Brangwynne, C.P. (2017). Liquid phase condensation in cell physiology and disease. Science *357*, eaaf4382.

Singleton, A., Farrer, M., Johnson, J., et al. (2003). α-synuclein locus triplication causes Parkinson's disease. Science *302*, 841.

Sinnige, T., Meisl, G., Michaels, T.C.T., et al. (2020). Kinetic analysis reveals the rates and mechanisms of protein aggregation in a multicellular organism. bioRxiv, https://doi.org/10.1101/2020.08.13.249862

Spillantini, M.G., Crowther, R.A., Jakes, R., et al. (1998). α-synuclein in filamentous inclusions of Lewy bodies from Parkinson's disease and dementia with Lewy bodies. Proc. Natl Acad. Sci. USA *95*, 6469–6473.

Spillantini, M.G., Schmidt, M.L., Lee, V.M.-Y., et al. (1997). α-synuclein in Lewy bodies. Nature *388*, 839–840.

Takamori, S., Holt, M., Stenius, K., et al. (2006). Molecular anatomy of a trafficking organelle. Cell *127*, 831–846.

Taschenberger, G., Garrido, M., Tereshchenko, Y., et al. (2012). Aggregation of α-synuclein promotes progressive in vivo neurotoxicity in adult rat dopaminergic neurons. Acta Neuropathol. *123*, 671–683.

Valera, E., and Masliah, E. (2016). Therapeutic approaches in Parkinson's disease and related disorders. J. Neurochem. *139*, 346–352.

Van Ham, T.J., Thijssen, K.L., Breitling, R., et al. (2008). C. elegans model identifies genetic modifiers of α-synuclein inclusion formation during aging. PLoS Genet. *4*, e1000027.

Visanji, N.P., Brotchie, J.M., Kalia, L.V., et al. (2016). α-synuclein-based animal models of Parkinson's disease: challenges and opportunities in a new era. Trends Neurosci. *39*, 750–762.

Volpicelli-Daley, L.A., Luk, K.C., and Lee, V.M. (2014). Addition of exogenous α-synuclein preformed fibrils to primary neuronal cultures to seed recruitment of endogenous α-synuclein to Lewy body and Lewy neurite-like aggregates. Nat. Protoc. *9*, 2135–2146.

Wakabayashi, K., Tanji, K., Odagiri, S., et al. (2013). The Lewy body in Parkinson's disease and related neurodegenerative disorders. Mol. Neurobiol. *47*, 495–508.

Warren, S.C., Margineanu, A., Alibhai, D., et al. (2013). Rapid global fitting of large fluorescence lifetime imaging microscopy datasets. PLoS One *8*, e70687.

Wegmann, S., Eftekharzadeh, B., Tepper, K., et al. (2018). Tau protein liquid–liquid phase separation can initiate tau aggregation. EMBO J. *37*, e98049.

Wilhelm, B.G., Mandad, S., Truckenbrodt, S., et al. (2014). Composition of isolated synaptic boutons reveals the amounts of vesicle trafficking proteins. Science *344*, 1023–1028.

Yuan, C., Levin, A., Chen, W., et al. (2019). Nucleation and growth of amino acid and peptide supramolecular polymers through liquid–liquid phase separation. Angew. Chem. Int. Ed. *131*, 18284–18291.

Zaltieri, M., Grigoletto, J., Longhena, F., et al. (2015). α-synuclein and synapsin III cooperatively regulate synaptic function in dopamine neurons. J. Cell Sci. *128*, 2231–2243.